Spin structure of the nucleon: QCD evolution, lattice results and models

4 authors:

Michael Altenbuchinger
Universitätsmedizin Göttingen
69 PUBLICATIONS 546 CITATIONS

SEE PROFILE

Philipp Haegler
Private Sector
155 PUBLICATIONS 4,383 CITATIONS

SEE PROFILE

Wolfram Weise
Technische Universität München
435 PUBLICATIONS 22,538 CITATIONS

SEE PROFILE

E. M. Henley
University of Washington Seattle
158 PUBLICATIONS 3,202 CITATIONS

SEE PROFILE

Spin structure of the nucleon:
QCD evolution, lattice results and models

M. Altenbuchinger,[a,1] Ph. Hägler,[a,b,2] W. Weise,[a,3] E. M. Henley[c]

[a]Physik Department, Technische Universität München, D-85747 Garching, Germany
[b]Institut für Theoretische Physik, Universität Regensburg, D-93040 Regensburg, Germany
[c]Dept. of Physics, University of Washington, Seattle, WA 98195-1560, USA

Abstract

The question how the spin of the nucleon is distributed among its quark and gluon constituents is still a subject of intense investigations. Lattice QCD has progressed to provide information about spin fractions and orbital angular momentum contributions for up- and down-quarks in the proton, at a typical scale $\mu^2 \sim 4\,\text{GeV}^2$. On the other hand, chiral quark models have traditionally been used for orientation at low momentum scales. In the comparison of such model calculations with experiment or lattice QCD, fixing the model scale and the treatment of scale evolution are essential. In this paper, we present a refined model calculation and a QCD evolution of lattice results up to next-to-next-to-leading order. We compare this approach with the Myhrer-Thomas scenario for resolving the proton spin puzzle.

[1]altenb@ph.tum.de
[2]phaegler@ph.tum.de
[3]weise@ph.tum.de

1 Introduction

How is the total spin 1/2 of the nucleon distributed among its quark and gluon constituents? This question has been intensely discussed ever since the EMC experiment presented first results for the spin asymmetry in polarized muon proton scattering in 1987 [1]. This measurement indicated that only about 15% or less of the nucleon spin is built up by quark spins, although with sizeable statistical and systematic uncertainties. Indeed, more recent measurements of HERMES and COMPASS [2, 3] and their QCD analysis [4–6] showed that the nucleon receives still only about one third of its spin from quark spins:

$$\Delta\Sigma_{\text{HERMES}}(5\text{GeV}^2) = 0.330 \pm 0.011_{\text{theo.}} \pm 0.025_{\text{exp.}} \pm 0.028_{\text{evol.}}, \tag{1}$$

determined at a scale $\mu^2 = 5\text{GeV}^2$. This is in stark contrast to naive model calculations, as for example in the non-relativistic quark model that suggests $\Delta\Sigma = 1$. Relativistic effects reduce $\Delta\Sigma$ to about two thirds, still far too large in comparison with Eq. (1). Myhrer and Thomas proposed in [7–10] that $\Delta\Sigma$ could be further reduced by including pion cloud contributions and corrections from one gluon exchanges. With such corrections they end up with a result for $\Delta\Sigma$ that is consistent with experiment. The missing $\approx 60 - 70\%$ of the nucleon spin reappear entirely as orbital angular momentum of up and down quarks L_{u+d}. On the other hand it turns out that this is in strong contrast to lattice calculations [11–13] where the orbital angular momentum contribution L_{u+d} comes out close to zero [13]. To explain this difference, Thomas [8] proposed to consider the renormalization scale (μ-)dependence of the quantities appearing in the nucleon spin sum rule [14]

$$\frac{1}{2}\Delta\Sigma + L_q + L_g + \Delta G = \frac{1}{2}, \tag{2}$$

defined by the following expectation values taken for a spin-up state of the proton, $|P+\rangle$:

$$\begin{aligned}
\Delta\Sigma &= \langle P + | \int d^3x \bar{\psi}\gamma^3\gamma_5\psi|P+\rangle, \\
\Delta G &= \langle P + | \int d^3x (E^1 A^2 - E^2 A^1)|P+\rangle, \\
L_q &= \langle P + | \int d^3x i\bar{\psi}\gamma^0(x^1\partial^2 - x^2\partial^1)\psi|P+\rangle, \\
L_g &= \langle P + | \int d^3x E^i(x^2\partial^1 - x^1\partial^2)A^i|P+\rangle.
\end{aligned} \tag{3}$$

Here ψ is the quark field, E^i and A^μ are the gluon electric field and gauge potential. A sum over quark flavors is implicit in the definition of the flavor singlet quantities in Eq. (3), and contributions in the non-singlet sector will be denoted by $\Delta\Sigma_{u-d}$, L_{u-d} etc. . The L_g is the orbital angular momentum contribution from gluons and ΔG is the gluon spin part. It is important to note that L_q, L_g and ΔG in Eq. (3) are not explicitly gauge invariant. A manifestly gauge invariant decomposition and its relation to moments of

generalized parton distributions was presented by Ji in [15, 16]:

$$\frac{1}{2}\Delta\Sigma + L_q^{\mathrm{GI}} + J_g^{\mathrm{GI}} = \frac{1}{2},$$ (4)

where $\Delta\Sigma$ is given as before, L_q^{GI} is obtained from L_q replacing ∂^μ by the gauge-covariant derivative, $\partial^\mu \to D^\mu$, and the total gluon angular momentum is defined as

$$J_g^{\mathrm{GI}} = \langle P + | \int d^3x [\vec{x} \times (\vec{E} \times \vec{B})]_3 | P+ \rangle .$$ (5)

Using a leading order QCD evolution of the spin contributions from the low, hadronic model scale to the higher scale of the lattice results, it was shown in Ref. [8] that it is possible to find at least a qualitative agreement with the lattice data.

With these previous achievements in mind, the purpose of the present work is twofold: first, we extend the QCD evolution to next-to-leading (NLO) and next-to-next-to-leading (NNLO) order and perform a backwards evolution starting from lattice results. This approach has the advantage that the scale dependence of the spin contributions is rather weak at the higher scale of lattice results, and that the extrapolation therefore does not suffer from the uncertainty of the slope in μ at low scales. Most importantly, proceeding in this way we do not have to fix the model scale a priori, which is generically difficult, but have the possibility to compare model results over a wider range of low scales with the downward-evolved lattice data. As a further extension, we use not only the perturbative coupling $\alpha_s(\mu)$ in the evolution equations but employ also a frequently suggested "non-perturbative" strong coupling that approaches a constant $\alpha_{s,\mathrm{max}}^{\mathrm{eff}}$ in the infrared region.

The second purpose of this work is to reexamine the model calculations of [7–10] and also to study possible improvements (chapter 3). Given these results and the evolved lattice data, we conclude with a discussion in chapter 4.

2 QCD evolution of lattice results

In this section we aim to evolve results from lattice QCD, usually provided in the $\overline{\mathrm{MS}}$ scheme at a scale $\mu^2 \simeq 4$ GeV^2, down to the low scales characteristic of model calculations. The lattice calculations were performed on the basis of manifestly gauge invariant operators. The computations correspond to the spin decomposition proposed by Ji, Eq. (4). For the remainder of this section, we will therefore employ the gauge invariant definitions of the spin observables. We drop the superscript GI in the following for better readability. To obtain the complete set of evolution equations for all individual parts of the spin sum rule, we define the orbital angular momentum of quarks as $L_q = J_q - \frac{1}{2}\Delta\Sigma$, of gluons as $L_g = J_g - \Delta G$ (for discussions of the latter definition, see refs. [16–18]).

Note that the gauge invariant ΔG cannot be represented in terms of a local operator [19], but can be defined as the lowest x-moment of the gauge invariant gluon spin distribution, $\Delta g(x)$. Despite remarkable experimental and theoretical efforts with respect to polarized PDFs [4–6, 20, 21], little is known so far about the magnitude of

a_1	b_1	d_1
$\frac{11744}{243}$	$\frac{416}{81}$	$\frac{611}{81}$

a_2	b_2	c_2	d_2	e_2
$\frac{5514208}{6561} + \frac{1280}{81}\zeta(3)$	$\frac{134888}{2187} + \frac{2560}{27}\zeta(3)$	$\frac{1136}{243}$	$\frac{670871}{4374} - \frac{2600}{27}\zeta(3)$	$\frac{8830}{729}$

Table 1: Coefficients entering the evolution equations (7).

ΔG. Concerning the numerical evaluation of the evolution equations, we will therefore concentrate on the quark spin, the quark orbital angular momentum and the total angular momentum of the gluons. As will be shown below, this can be done without explicit knowledge about ΔG and $L_g = J_g - \Delta G$. It then follows that the evolution of all quantities of interest can also be performed at NNLO, employing known results for the relevant anomalous dimensions from the literature.

The total angular momentum contributions J_q and J_g are introduced as in [16] in the framework of generalized parton distributions. We observe that J_q and J_g mix in exactly the same way under renormalization as the (symmetric and traceless) quark and gluon energy momentum tensors. This can be seen for example by rewriting

$$\langle P,s|J_{q,g}^i|P,s\rangle = \frac{1}{2}\epsilon_{ijk}\lim_{\Delta^\mu \to 0}\left[-i\frac{\partial}{\partial\Delta^i}\langle P+\frac{\Delta}{2},s|T_{q,g}^{0k}|P-\frac{\Delta}{2},s\rangle + \left\{j \leftrightarrow k\right\}\right](2\pi)^3\delta(\vec{\Delta}). \quad (6)$$

Here, the additional derivative with respect to the momentum transfer, Δ^μ, cannot have any influence on the singular behavior of the operators. Therefore they mix in the same manner. The QCD evolution equations for J_q and J_g are constructed using the spin-2 singlet anomalous dimension given at next-to-leading order in [22, 23] and at next-to-next-to-leading order in [24–26].This yields

$$\frac{d}{d\ln\mu^2}\begin{pmatrix} J_q \\ J_g \end{pmatrix} = -\frac{\alpha_s}{4\pi}\begin{pmatrix} \frac{32}{9} & -\frac{2}{3}n_F \\ -\frac{32}{9} & \frac{2}{3}n_F \end{pmatrix}\begin{pmatrix} J_q \\ J_g \end{pmatrix}$$
$$-\left(\frac{\alpha_s}{4\pi}\right)^2\begin{pmatrix} a_1 - b_1 n_F & -d_1 n_F \\ -a_1 + b_1 n_F & d_1 n_F \end{pmatrix}\begin{pmatrix} J_q \\ J_g \end{pmatrix}$$
$$-\left(\frac{\alpha_s}{4\pi}\right)^3\begin{pmatrix} a_2 - b_2 n_F - c_2 n_F^2 & -d_2 n_F + e_2 n_F^2 \\ -a_2 + b_2 n_F + c_2 n_F^2 & d_2 n_F - e_2 n_F^2 \end{pmatrix}\begin{pmatrix} J_q \\ J_g \end{pmatrix} \quad (7)$$

for n_F flavours (compare also [27]), with entries $a_i, b_i, ...$ given in Table 1. For the non-singlet combination J_q^{NS}, we find

$$\frac{d}{d\ln\mu^2}J_q^{NS} = -\frac{\alpha_s}{4\pi}\frac{32}{9}J_q^{NS} - \left(\frac{\alpha_s}{4\pi}\right)^2\left(\frac{11744}{243} - \frac{256}{81}n_F\right)J_q^{NS}$$
$$-\left(\frac{\alpha_s}{4\pi}\right)^3\left(\frac{5514208}{6561} + \frac{1280\,\zeta(3)}{81} - \frac{167200\,n_F}{2187} - \frac{1280\,n_F\,\zeta(3)}{27} - \frac{896\,n_F^2}{729}\right)J_q^{NS}.$$
$$(8)$$

4

The evolution equations for the spin contributions at NNLO in the MS($\overline{\text{MS}}$) scheme [28], [29] (these two schemes are simply connected through a change in the renormalization scale) are given by [30–32]

$$\frac{d}{d\ln\mu^2}\begin{pmatrix}\Delta\Sigma\\\Delta G\end{pmatrix} = -\frac{\alpha_s}{4\pi}\begin{pmatrix}0 & 0\\-4 & -\beta_0\end{pmatrix}\begin{pmatrix}\Delta\Sigma\\\Delta G\end{pmatrix} - \left(\frac{\alpha_s}{4\pi}\right)^2\begin{pmatrix}8n_F & 0\\-100+\frac{8}{9}n_F & -\beta_1\end{pmatrix}\begin{pmatrix}\Delta\Sigma\\\Delta G\end{pmatrix}$$
$$-\left(\frac{\alpha_s}{4\pi}\right)^3\begin{pmatrix}200n_F-\frac{16n_F^2}{9} & 0\\\gamma_{gq} & \gamma_{gg}\end{pmatrix}\begin{pmatrix}\Delta\Sigma\\\Delta G\end{pmatrix}. \tag{9}$$

At NNLO, the anomalous dimensions γ_{gq} and γ_{gg} are still unknown, while the upper row $(\gamma_{qq},\gamma_{qg})$ has been obtained as described in [32]. Here the QCD beta functions are

$$\beta_0 = 11 - \frac{2n_F}{3}, \qquad \beta_1 = 102 - \frac{38}{3}n_F. \tag{10}$$

We stress that in the chosen renormalization scheme, the evolution of $\Delta\Sigma$ is independent of ΔG, even at NNLO. Furthermore, since $J_q + J_g = 1/2$ at any scale, the evolution of J_q does not require an independent knowledge of the value of J_g. Hence one finds the remarkable result, already mentioned above, that neither ΔG nor $L_g = J_g - \Delta G$ are actually required in practice for the scale evolution of $L_q = J_q - \Delta\Sigma/2$. As a consequence the evolution of all the quantities in Eq. (4) can be performed at NNLO.

Employing the definitions of L_q and L_g given above, fully consistent coupled evolution equations for the orbital angular momenta of quarks and of gluons can be written,

$$\frac{d}{d\ln\mu^2}\begin{pmatrix}L_q\\L_g\end{pmatrix} = -\frac{\alpha_s}{4\pi}\begin{pmatrix}\frac{32}{9} & -\frac{2}{3}n_F\\-\frac{32}{9} & \frac{2}{3}n_F\end{pmatrix}\begin{pmatrix}L_q\\L_g\end{pmatrix} - \frac{\alpha_s}{4\pi}\begin{pmatrix}\frac{16}{9} & -\frac{2}{3}n_F\\\frac{20}{9} & 11\end{pmatrix}\begin{pmatrix}\Delta\Sigma\\\Delta G\end{pmatrix}$$
$$-\left(\frac{\alpha_s}{4\pi}\right)^2\begin{pmatrix}\frac{11744}{243}-\frac{416}{81}n_F & -\frac{611}{81}n_F\\-\frac{11744}{243}+\frac{416}{81}n_F & \frac{611}{81}n_F\end{pmatrix}\begin{pmatrix}L_q\\L_g\end{pmatrix}$$
$$-\left(\frac{\alpha_s}{4\pi}\right)^2\begin{pmatrix}\frac{5872}{243}-\frac{532}{81}n_F & -\frac{611}{81}n_F\\\frac{18428}{243}+\frac{136}{81}n_F & 102-\frac{415}{81}n_F\end{pmatrix}\begin{pmatrix}\Delta\Sigma\\\Delta G\end{pmatrix}, \tag{11}$$

at next-to-leading order in the MS($\overline{\text{MS}}$) scheme.

An overview of lattice QCD calculations of nucleon spin observables, in particular of moments of generalized parton distributions that give access to the total quark angular momentum J_q, can be found in [33]. Here we focus on the latest published results from the LHP collaboration [34]. They were obtained in the framework of a mixed action approach with $N_f = 2 + 1$ dynamical fermions, with lattice pion masses as low as ≈ 300 MeV. The computationally demanding quark line disconnected diagrams, which contribute in the singlet sector, were not included in this study. The final values for $\Delta\Sigma_q$, L_q and J_q at the physical pion mass were obtained from extrapolations employing the covariant baryon chiral perturbation theory results of [35]. We refer to the original

	$\Delta\Sigma/2$	L_q
u	0.411(36)	-0.175(36)(17)
d	-0.203(35)	0.205(35)(0)

Table 2: Lattice QCD results from Ref. [34] for the proton spin observables in the $\overline{\text{MS}}$ scheme at $\mu^2 = 4\,\text{GeV}^2$, separated into u- and d-quark contributions. Statistical and estimated systematic uncertainties due to the renormalization are given in the form $(\ldots)_{\text{stat}}(\ldots)_{\text{ren}}$.

publication [34] for the details of the lattice simulation, the numerical analysis, and a discussion of the statistical and systematic uncertainties. A summary of the lattice results, for the $\overline{\text{MS}}$ scheme at a scale of $4\,\text{GeV}^2$, is given in table 2. The errors given in this table do not include systematic uncertainties from chiral extrapolations and disconnected diagrams.

For our extrapolation of lattice results, we assume a vanishing contribution from strange quarks. The total gluon angular momentum is given by $J_g = \frac{1}{2} - J_{u+d}$. Using this value with $\Delta\Sigma$ and L_q given in Table 2 as starting points, and setting $n_F = 3$ and $\Lambda_{\overline{\text{MS}}}^{(3)} = 338\,\text{MeV}$ [36], we have solved the coupled evolution equations and found the scale dependence plotted in Figures 1 and 2.

The results at LO, NLO and NNLO, employing the standard analytical expressions for the perturbative strong coupling constant (corresponding to an expansion in $1/\ln(\mu^2/\Lambda^2)$ beyond LO, see, e.g., [37]) in the $\overline{\text{MS}}$ scheme at the appropriate order, are given by the short-dashed, dashed, and solid thin black curves, respectively. Clearly, the deviation of the approximate analytical expressions for α_s from the exact (numerical) solutions of the evolution equations increases as one approaches lower scales. We note that for $n_F = 3$ and $\Lambda_{\overline{\text{MS}}}^{(3)} = 338\,\text{MeV}$, the formally exact solution for the running coupling at NNLO would already diverge around $\mu^2 \sim 0.3\,\text{GeV}^2$. The curves in Fig. 1 obtained for α_s in the $1/\ln$-approximation are therefore only indicative for a strong coupling constant that grows indefinitely as $\mu^2 \to 0$.

More generally, a comparison with the model results, e.g. as proposed by Myhrer and Thomas [7–10], requires an evolution down to scales $\mu^2 \sim 0.1 - 0.3\,\text{GeV}^2$, far away from the perturbative QCD regime. Obviously at such low scales quantitative statements based on a perturbative QCD analysis (including the running of α_s) are not reliable. The large gap between the results at NLO and NNLO for $\mu^2 \sim 0.1 - 0.3\,\text{GeV}^2$ provides already a first idea about the size of the corresponding uncertainties.

With respect to (the non-perturbative) α_s, one would expect in any case that it saturates at low scales, as suggested by non-perturbative resummation in the infrared region [38–40]. A further rough impression about the uncertainties in the evolution may therefore be obtained as follows. As an alternative to the infrared divergent, perturbative coupling $\alpha_s(\mu^2)$ in the evolution equations, use an effective $\alpha_s^{\text{eff}}(\mu)$ that approaches a fixed value $\alpha_{s,\text{max}}^{\text{eff}}$ at small μ^2. For the corresponding numerical calculation we have used $\alpha_s^{\text{eff}}(\mu^2) = \alpha_s(\mu^2)$ of appropriate order in the $\overline{\text{MS}}$ scheme for all μ for which $\alpha_s(\mu^2) \leqslant \alpha_{s,\text{max}}^{\text{eff}}$. Below the scale μ_0 at which $\alpha_s(\mu_0^2) = \alpha_{s,\text{max}}^{\text{eff}}$, we use $\alpha_s^{\text{eff}} \equiv \alpha_{s,\text{max}}^{\text{eff}}$. The
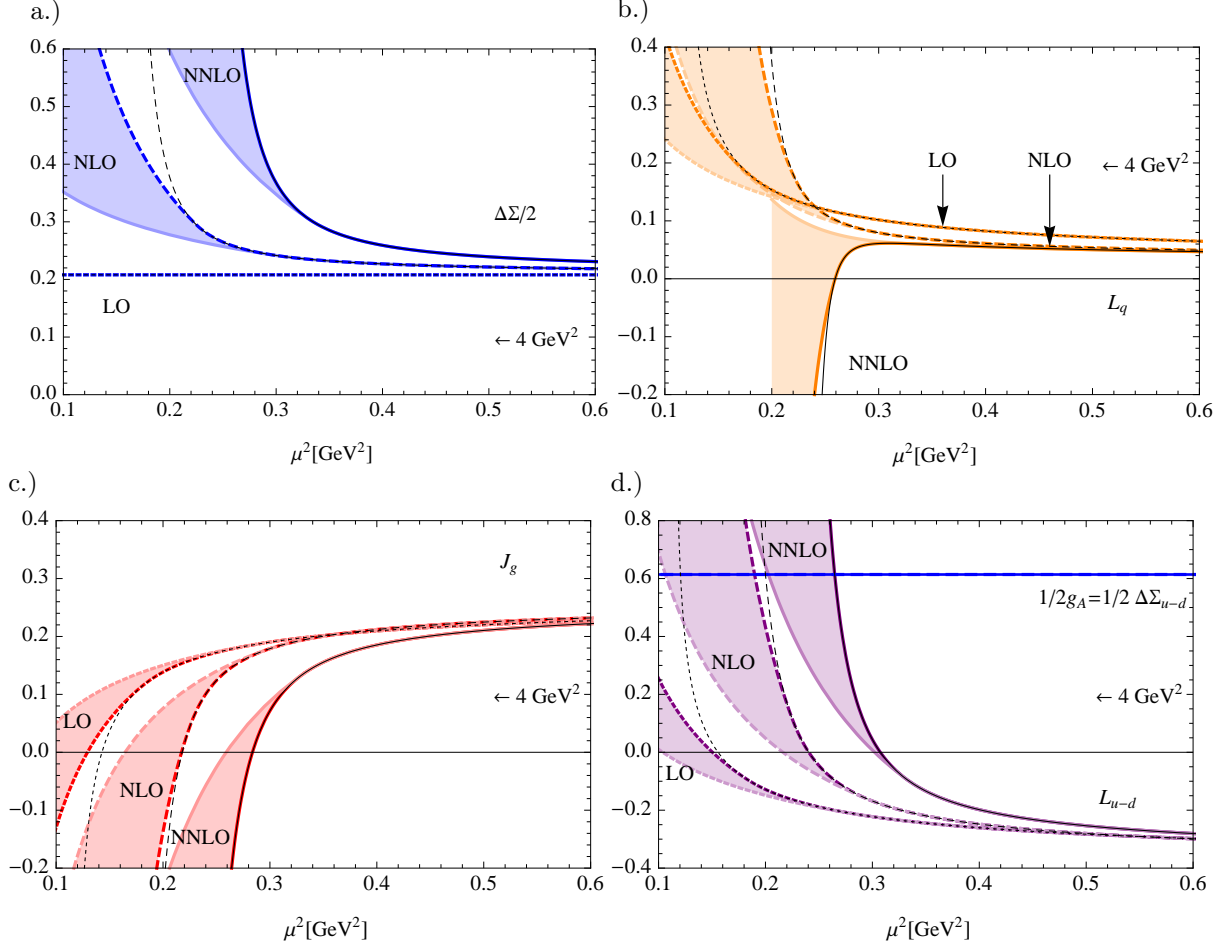
Figure 1: Scale dependence of $\Delta\Sigma/2$, L_q, J_g, and L_{u-d} shown together with $\frac{1}{2}g_A = \frac{1}{2}\Delta\Sigma_{u-d}$, starting from the lattice QCD results at $\mu^2 = 4\,\text{GeV}^2$ given in table 2. In all diagrams the solid, dashed and short-dashed lines are solutions of the QCD evolution equations at NNLO, NLO, and LO, respectively. The evolution using the perturbative $\overline{\text{MS}}$ coupling is given by the black lines. The colored thick lines are obtained by using α_s bounded from above (see text), where the darker colored lines correspond to the bound $\alpha_{s,\text{max}}^{\text{eff}} = 3$ and the lighter colored lines to $\alpha_{s,\text{max}}^{\text{eff}} = 1.5$.

corresponding results are represented in Figures 1 and 2 by the darker colored lines for $\alpha_{s,\text{max}}^{\text{eff}} = 3$, and by the lighter colored lines for $\alpha_{s,\text{max}}^{\text{eff}} = 1.5$. The region in between these two cases is highlighted by the shaded bands.

The most important fact to realize is that L_q evolves towards larger positive values in LO and NLO at low scales, but towards negative values at NNLO (solid black line in Fig. 1b). The qualitative behavior of L_{u-d} (see Fig. 1d) at low scales persists instead at all orders considered: L_{u-d} evolves from sizable negative values at $\mu^2 = 4\,\text{GeV}^2$ to positive values at low scales. Interestingly, the separate evolution of L_u and L_d (see Fig. 2) remains qualitatively the same at all considered orders. Both L_u and L_d tend to change sign as they evolve towards small scales. One realizes that the crossing point of L_u and L_d moves downwards, going from LO to NLO to NNLO. The zero-crossing points, on the other hand, move towards larger μ^2 when going to higher orders in the
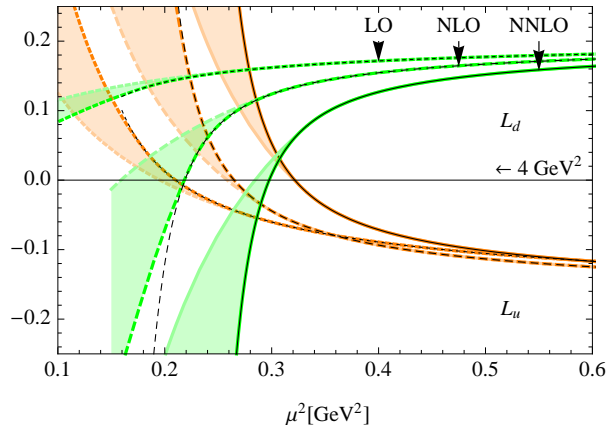
Figure 2: Evolution of L_u and L_d in NNLO (solid lines), NLO (dashed lines) and LO (short dashed lines). The colors and shaded areas are assigned as in Fig.1.

evolution equations. A more detailed discussion, especially of the influence of a cutoff $\alpha_{s,\max}^{\mathrm{eff}}$, and a comparison of evolved lattice results with calculations performed in a chiral quark model, follows in section 4.

3 Contributions to the nucleon spin in a chiral quark model

3.1 Pion cloud contributions, revisited

It is a well established fact that the nucleon is a complex many-body system, with the three valence quarks and multiple quark-antiquark pairs embedded in a strong, non-perturbative gluonic field configuration. Chiral quark models draw a simplified picture of this complexity in terms of valence quarks in a confining bag coupled to the pion cloud, based on spontaneously broken chiral symmetry in low-energy QCD. A frequently used representative of such chiral models is the cloudy bag (CBM) [41–43] that couples the pion cloud to quarks in the MIT bag [44] such that chiral invariance is realized in the limit of massless quarks. This section summarizes the present status concerning nucleon spin structure from this model point of view.

The relativistic treatment of quarks itself yields already results that differ significantly from the ordinary SU(6) quark model predictions. The $\Delta\Sigma = 1$ of the non-relativistic quark model is reduced to about $\Delta\Sigma^{\mathrm{MIT}} = 0.65$ in the MIT bag model. The "missing spin" is interpreted as orbital angular momentum of the valence quarks, $2L_{u+d}^{\mathrm{MIT}} = 0.35$, associated with the lower components of the Dirac quark wave functions.

The correction factors for the pion cloud in the CBM were already derived by Myhrer and Thomas in [7–10]. For the singlet expectation values,

$$\Delta\Sigma^{\mathrm{CBM}} = 0.65 \cdot \Pi_{\mathrm{S}}(R), \qquad 2L_q^{\mathrm{CBM}} = 0.35 \cdot \Pi_{\mathrm{S}}(R), \qquad 2L_\pi^{\mathrm{CBM}} = 1 - \Pi_{\mathrm{S}}(R), \quad (12)$$

8
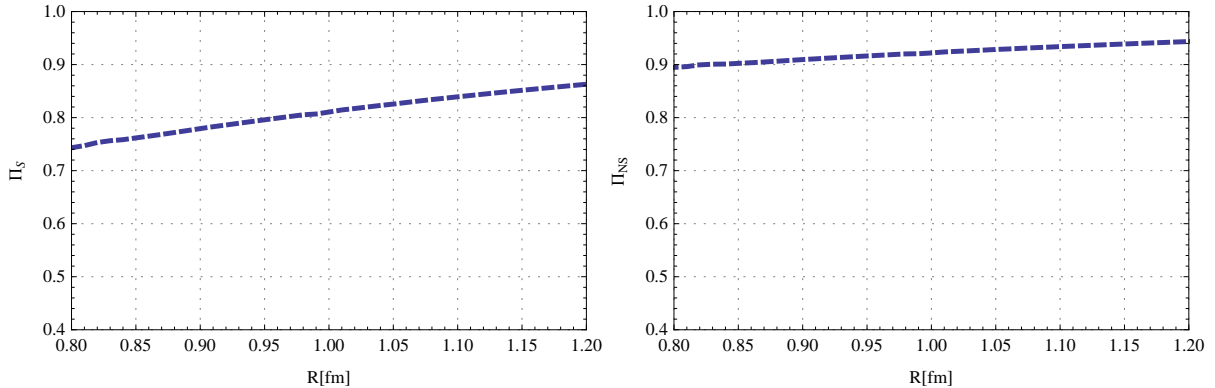
Figure 3: Radius dependence of the singlet and non-singlet corrections Π_S and Π_{NS} associated with the pion cloud of the nucleon.

and for the non-singlet expectation values [45],

$$\Delta\Sigma_{u-d}^{CBM} = g_A^{(3)\,CBM} = \frac{5}{3} \cdot 0.65 \cdot \Pi_{NS}(R), \qquad 2L_{u-d}^{CBM} = \frac{5}{3} \cdot 0.35 \cdot \Pi_{NS}(R). \qquad (13)$$

We have denoted the pion cloud correction factors by $\Pi_S(R)$ and $\Pi_{NS}(R)$, each for a given bag radius R. For their explicit form we refer to [7–10,45] and references therein. Notice that the value $g_A^{(3)} = 1.27$, given in [7–10], is obtained by adjusting a phenomenological center-of-mass correction (which has however not been included for any of the other spin observables [45]).

We have reproduced the results (12) and (13) using the formalism described in [43]. The radius dependence of the correction factors is plotted in Figure 3. The singlet correction factor, Π_S, is smaller than unity and hence leads to the expected reduction of the quark spin contribution. At the same time, $\Pi_{NS} < 1$ leads to a slightly less favourable comparison of $g_A^{(3)\,CBM}$ with the experimental value of g_A (not taking into account the center-of-mass correction mentioned above).

3.2   Corrections from one-gluon exchange processes

The MIT bag model produces degenerate masses of the nucleon and the delta, whereas the empirical mass splitting is about 300MeV. In order to account for this mass difference, an additional spin-spin interaction between quarks is introduced. The common way to do this is to allow for quark-gluon interactions in the interior of the bag. The results depend on the strong coupling constant, α_s, treated as a free parameter of the model. In [46], a value of $\alpha_s = 2.2$ was chosen to fit the baryon spectrum at leading order. At order α_s^2 [47], the best fit could be obtained using $\alpha_s = 1$. In both calculations, only pure gluon exchange diagrams were calculated and all divergent loop diagrams were neglected.

We have performed calculations in analogy to ref. [48], where the color magnetic corrections to baryon magnetic moments and to semileptonic decays, i.e. the axial coupling constant, were derived at order α_s. Following the arguments given there, we
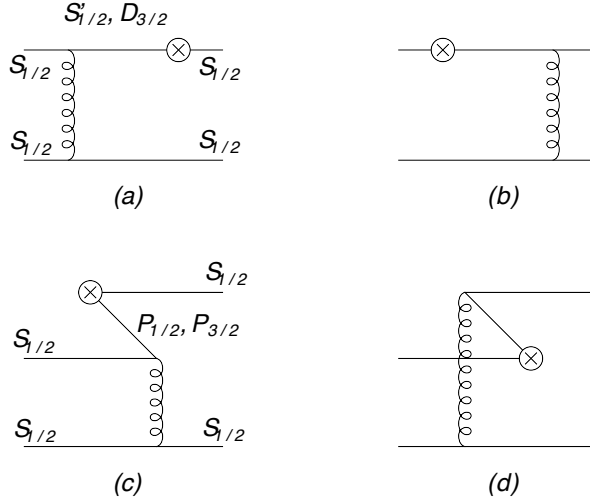
Figure 4: One-gluon exchange (OGE) corrections for $\Delta\Sigma$, $L_{S,NS}$ and $g_A^{(3)}$. Diagram (a) and (b) are contribution from intermediate quark states and (c) and (d) from quark-antiquark pairs.

neglect the color electric corrections and drop loop diagrams. That means, we consider diagrams 4(a)-4(d), in which only color magnetic gluons are exchanged.

For the singlet expectation values, $\Delta\Sigma$ and L_q, we find the (additive) OGE corrections

$$\delta\Delta\Sigma = -2\delta_g \cdot \alpha_s, \qquad \delta L_q = \delta_g \cdot \alpha_s, \tag{14}$$

with $\delta_g \simeq 2.5 \cdot 10^{-2}$, where L_q is used in its non-gauge-invariant formulation (3), and intermediate (anti-)quarks in the orbitals $P_{1/2}, P_{3/2}, D_{3/2}, S'_{1/2}, P'_{1/2}, P'_{3/2}, D'_{3/2}, S''_{1/2}$ are taken into account (conventions are chosen as in [48]). As already pointed out in [7–10] the corrections are mainly due to antiquarks propagating in the $P_{1/2}, P_{3/2}$ orbitals. Compared to $\delta\Delta\Sigma \sim -0.15$ and $\delta L_q \sim 0.08$ for $\alpha_s = 2.2$ as presented in [9], our corrections are slightly smaller.

For the non-singlet operators we find:

$$\delta\Delta\Sigma_{u-d} = \delta g_A^{(3)} = \frac{2}{3}\delta_g \cdot \alpha_s, \qquad \delta L_{u-d} = -\frac{1}{3}\delta_g \cdot \alpha_s. \tag{15}$$

The correction $\delta g_A^{(3)}$ is in agreement with [49]. However, δL_{u-d} differs in magnitude and sign from the result given in [8]. In order to understand a possible cause of this discrepancy, we first note that in our calculation, δL_{u-d} ends up with a factor $\langle p \uparrow | \sum_{i \neq j} \sigma_z(i)\tau_z(j)|p \uparrow\rangle$, where the operators are applied to different quark currents i and j. This is just what happens in the correction for g_A (where we do find agreement). Interestingly, the result of [8] for δL_{u-d} could be reproduced instead if we would perform the translation from the singlet case, i.e. δL_q, in [8] to the non-singlet expectation values by replacing $\langle p \uparrow | \sum_i \sigma_z(i)|p \uparrow\rangle \rightarrow \langle p \uparrow | \sum_i \sigma_z(i)\tau_z(i)|p \uparrow\rangle = \frac{5}{3}$, i.e. an expression where quark current indices are (wrongly) summed over one and the same index.

Explicit numbers for the singlet and non-singlet contributions to the nucleon spin in the MIT bag model, as well as the OGE-improved MIT bag and cloudy bag model, for two different values of α_s, are displayed in Table 3.

10

	$\Delta\Sigma/2$	L_q	$\Delta\Sigma_{u-d}/2$	L_{u-d}
relativistic (MIT bag model)	0.33	0.17	0.54	0.29
+OGE (α_s=1.0):	0.30	0.20	0.55	0.28
(α_s=2.2):	0.27	0.23	0.56	0.27
+pion cloud ($R = 1$fm, α_s=1.0):	0.24	0.26	0.51	0.26
($R = 1$fm, α_s=2.2):	0.22	0.28	0.52	0.25

Table 3: Spin structure of the nucleon in the MIT bag model, with corrections from one-gluon exchanges (OGE), and from the pion cloud. The non-gauge-invariant decomposition of the nucleon spin, Eqs. (3), is used here.
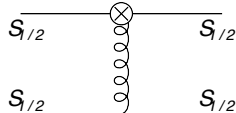
Figure 5: One-gluon exchange diagram attached to a quark-quark-gluon interaction vertex.

Once explicit gluon degrees of freedom, e.g. in form of one gluon exchange processes, are taken into account, the questions of gauge invariance of the calculation must be carefully addressed. For a consistent calculation that includes gluon exchange contributions at order α_s, and for a meaningful comparison with results from lattice QCD, we have to employ the gauge-invariant orbital angular momentum operator L_q^{GI} in Eq. (4) instead of L_q defined in (3). Due to the covariant derivative in L_q^{GI}, an additional quark-gluon interaction term appears, so that one must take into account the diagram in Fig. 5 for the corrections at order α_s to the MIT bag expectation values. This diagram yields the large contribution

$$\delta L_{q,A} = 0.203\,\alpha_s\,, \tag{16}$$

where the subscript A stands for the gauge field interaction term. The total correction to the quark orbital momentum is then given by $\delta L_q^{\mathrm{GI}} = \delta L_q + \delta L_{q,A}$. The diagram in Fig. 5 also contributes to the gauge invariant L_{u-d}^{GI} and shifts it by

$$\delta L_{u-d,A} = -\frac{1}{3}\delta L_{q,A}. \tag{17}$$

Furthermore, from the gauge-invariant spin sum rule Eq. (4), we conclude that the contribution from the total gluon angular momentum equals

$$J_g^{\mathrm{GI}} = -\delta L_{q,A}. \tag{18}$$

We notice that the corrections (16)-(18) are much larger than the known one-gluon exchange contributions from the diagrams of Fig. 4 given in Eqs. (14), (15). In particular, $\delta L_{q,A}$ dominates L_q^{MIT} for the chosen parameters. The MIT bag model results for the gauge invariant decomposition of the nucleon spin are summarized in Table 4, together with the combined results, including relativistic effects plus (full) one-gluon exchange corrections plus corrections from the pion cloud.

	$\Delta\Sigma/2$	L_q^{GI}	J_g^{GI}	$\Delta\Sigma_{u-d}/2$	L_{u-d}^{GI}
relativistic (MIT bag model)	0.33	0.17	0	0.54	0.29
+OGE (α_s=1.0):	0.30	0.40	-0.20	0.55	0.21
(α_s=2.2):	0.27	0.68	-0.45	0.56	0.12
+pion cloud ($R = 1$fm, α_s=1.0):	0.24	0.42	-0.16	0.51	0.19
($R = 1$fm, α_s=2.2):	0.22	0.64	-0.36	0.52	0.10

Table 4: Spin structure of the nucleon, based on manifestly gauge invariant operators, in the MIT bag model, together with corrections from one gluon exchanges (OGE) and from the pion cloud.

To conclude this section, we emphasize that a direct calculation of $J_g^{\mathrm{GI}} = \langle P+ | \int d^3r[\vec{r} \times (\vec{E} \times \vec{B})]_3 |P+\rangle$ (i.e. not invoking the spin sum rule) in the framework of the model requires a careful treatment of the boundary conditions for the color electric fields. The boundary conditions $\hat{\vec{r}} \cdot \vec{E}|_{r=R}$ cannot be fulfilled for the color electric fields, in the way described in [50]. This leads to a non-vanishing surface term in the calculation of J_g^{GI} and, therefore, potentially to inconsistencies with respect to the spin sum rule. A calculation with color electric fields that obey the boundary conditions, as given in [51], turns out to be significantly more involved and will not be described in this work. Note, however, that $\delta L_{q,A}$ is not affected by such complications since the corresponding operator does not involve color electric fields. It is therefore legitimate to extract the corresponding gluon angular momentum from $J_g^{\mathrm{GI}} = 1/2 - J_q^{\mathrm{GI}} = -\delta L_{q,A}$.

When J_g^{GI} is calculated directly, using the "wrong" color electric fields, it spoils the spin sum rule. Actually the direct evaluation of J_g^{GI} can be used to check our result for $\delta L_{q,A}$. Consider the decomposition

$$\int d^3r\, \vec{r} \times (\vec{E} \times \vec{B}) = \int d^3x\, \vec{E} \times \vec{A} + \int d^3x\, E^i(\vec{x} \times \nabla)A^i \qquad (19)$$

$$- \int d^3x\, g\psi^\dagger(\vec{x} \times \vec{A})\psi - \int d^3x\nabla^j[E^j(\vec{x} \times \vec{A})]. \qquad (20)$$

The left hand side corresponds to J_g^{GI}, the right hand side to $\Delta G + L_g - \delta L_{q,A}$ supplemented by a surface term, $-\int d^3x\nabla^j[E^j(\vec{x} \times \vec{A})]$. This surface terms vanishes in the free field theory but in our model calculation this is not the case. Therefore, the total gluon angular momentum calculated through the spin sum rule equals $\int d^3r\, \vec{r} \times (\vec{E} \times \vec{B}) + \int d^3x\nabla^j[E^j(\vec{x} \times \vec{A})]$, which indeed can be confirmed by a direct calculation. In fact, the OGE corrections to ΔG and L_g cancel each other.

4   Discussion and summary

The present study has been motivated by the observation of an apparent contradiction between quark orbital momentum contributions, L_q and L_{u-d}, calculated in models and derived from lattice QCD computations. At the same time, results from models and lattice QCD for the quark spin contributions $\Delta\Sigma$ and $g_A = \Delta\Sigma_{u-d}$ are reasonably consistent once pion cloud and gluon exchange effects are incorporated in the model [7].

Let us now discuss these features in more detail. Consider first the LO QCD evolution without imposing limiting constraints on α_s at low scales. From the short dashed black line in Fig.1b it is seen that the small lattice value for L_q evolves towards large positive values as one approaches low scales. The evolved lattice results would roughly match the model results at a small scale $\mu^2_{\mathrm{model}} \sim 0.14 - 0.16\,\mathrm{GeV}^2$. A similar observation is made for the non-singlet combination L_{u-d} (cf. Fig. 1d) that evolves from sizable negative to positive values which compare favorably with CBM results around μ^2_{model}. Since $\Delta\Sigma$ is scale independent at LO and g_A is scale independent to all orders, and the CBM results for $\Delta\Sigma$ as well as g_A are compatible with lattice QCD values, it might then appear that the aforementioned contradiction can be resolved. This was the point made in [8].

However, the matching scale μ^2_{model} is evidently far too small to draw any meaningful conclusions, in particular at LO. We have therefore extended the QCD evolution up to NNLO in order to examine the systematics. At NLO, $\Delta\Sigma$ becomes scale dependent and increases with lower scales, a behavior that is even more strongly enforced in NNLO. At the same time, the estimated matching scale at which model results are approached now increases to $\mu^2_{\mathrm{model}} \sim 0.22\,\mathrm{GeV}^2$ at NLO, and tends to increase further at NNLO. Incidentally, the NLO evolved lattice results turn out to be quite close to the original MIT bag values at $\mu^2_{\mathrm{model}} \sim 0.22\mathrm{GeV}^2$ where $J_g(\mu^2_{\mathrm{model}}) = 1/2 - L_{u+d} - \Delta\Sigma/2 \simeq 0$. As the model calculations are improved, however, this apparent consistency deteriorates. Inclusion of the pion cloud in the CBM lowers $\Delta\Sigma$ and increases L_q significantly. Further inclusion of gluon exchange corrections would make the matching with the evolved lattice data progressively more difficult.

Finally, consider the NNLO evolution. Except for L_q (see Fig. 1b), the qualitative features are similar to the NLO situation. At this point it is interesting to examine the effects of replacing the perturbative $\alpha_s(\mu^2)$ by an effective α_s that is constrained by a maximal value $\alpha^{\mathrm{eff}}_{s,\mathrm{max}}$ at small scales. Using upper bounds between $\alpha^{\mathrm{eff}}_{s,\mathrm{max}} \sim 3$ and $\alpha^{\mathrm{eff}}_{s,\mathrm{max}} \sim 1.5$ gives the borders of the shaded areas in Figs. 1, with particularly strong sensitivity observed in $L_q(\mu^2)$. For $\alpha^{\mathrm{eff}}_{s,\mathrm{max}} \sim 3$ this L_q moves from positive to negative as one approaches $\mu^2 \sim 0.25\,\mathrm{GeV}^2$ from above. On the other hand, L_q remains positive and flat throughout if $\alpha^{\mathrm{eff}}_{s,\mathrm{max}}$ is constrained not to exceed 1.5, indicating that such a scenario may improve the stability of the downward scale evolution.

Concerning the lattice calculations, one source of systematic uncertainty can be eliminated by studying isovector quantities such as L_{u-d} for which disconnected diagrams, not taken into account in Ref. [34], cancel out. From the model investigations (see Tables 3, 4) one expects $L^{(GI)}_{u-d}$ in the range of $0.1 - 0.3$.[1] In contrast, the lattice results start negative at $\mu^2 \sim 4\,\mathrm{GeV}^2$. The downward QCD evolution does predict the appropriate change of sign (see Fig. 1d) at all orders considered. The scale at which this sign change occurs, increases from $\mu^2 \sim 0.15\,\mathrm{GeV}^2$ to $0.25\,\mathrm{GeV}^2$ to about $\mu^2 \sim 0.3\,\mathrm{GeV}^2$ when going from LO to NLO to NNLO, bringing lattice results and model expectations into closer contact at scales where the evolution begins to be more reliable. Other systematic uncertainties on the lattice side, for example those related to lattice operator renormalization

---

[1]Note, however, that a recent calculation using a chiral quark soliton model gives a negative L_{u-d} even at low scales [52].

issues, would affect the normalization of L_{u-d} but would not change this picture significantly. In contrast to the singlet L_q, inclusion of explicit gluon degrees of freedom in the properly gauge invariant treatment of the quark orbital momentum operator leads to a reduction of L_{u-d} at model scales (see Tables 3, 4) and moves this quantity closer to the extrapolated lattice QCD results. The sign change of L_{u-d} can be traced in detail by examining the crossing of L_u and L_d as shown in Fig. 2.

In summary, our analysis underlines the difficulty of simultaneously understanding model calculations and lattice QCD results for the decomposition of the nucleon's spin into the angular momenta of the constituents. NNLO and NLO corrections turn out to be of similar magnitude at the relevant low scales, indicating (not unexpectedly) that reliable convergence is not reached in the evolution from lattice to low-energy models. Conversely, this implies that it is difficult to arrive at quantitatively reliable predictions from model calculations starting at scales smaller than $\mu^2 \sim 0.4\,\mathrm{GeV}^2$ and evolving upward to scales accessible in experiments and related QCD phenomenology.

A possible exception concerning this critical assessment is the isovector orbital angular momentum combination L_{u-d} for which systematic lattice errors are minimal. Unlike L_q, this quantity displays systematic behavior with a sign change as it evolves from lattice QCD to low scales, in accordance with the model expectations listed in Tables 3 and 4.

Acknowledgments

References

[1] J. Ashman *et al.* [European Muon Collaboration], Phys. Lett. B **206** (1988) 364.

[2] A. Airapetian *et al.* [HERMES Collaboration], Phys. Rev. D **75** (2007) 012007 [arXiv:hep-ex/0609039].

[3] V. Y. Alexakhin *et al.* [COMPASS Collaboration], Phys. Lett. B **647**, 8 (2007) [arXiv:hep-ex/0609038].

[4] J. Blümlein, H. Böttcher, Nucl. Phys. **B841** (2010) 205-230. [arXiv:1005.3113 [hep-ph]].

[5] D. de Florian, R. Sassot, M. Stratmann and W. Vogelsang, Phys. Rev. D **80** (2009) 034030 [arXiv:0904.3821 [hep-ph]].

[6] E. Leader, A. V. Sidorov and D. B. Stamenov, arXiv:1010.0574 [hep-ph].

[7] F. Myhrer and A. W. Thomas, Phys. Lett. B **663** (2008) 302 [arXiv:0709.4067 [hep-ph]].

[8] A. W. Thomas, Phys. Rev. Lett. **101** (2008) 102003 [arXiv:0803.2775 [hep-ph]].

[9] A. W. Thomas, Int. J. Mod. Phys. E **18** (2009) 1116 [arXiv:0904.1735 [hep-ph]].

[10] A. W. Thomas, Prog. Part. Nucl. Phys. **61** (2008) 219 [arXiv:0805.4437 [hep-ph]].

[11] P. Hägler, J. W. Negele, D. B. Renner, W. Schroers, T. Lippert and K. Schilling [LHPC collaboration and SESAM collaboration], Phys. Rev. D **68**, 034505 (2003) [arXiv:hep-lat/0304018].

[12] M. Göckeler, R. Horsley, D. Pleiter, P. E. L. Rakow, A. Schäfer, G. Schierholz and W. Schroers [QCDSF Collaboration], Phys. Rev. Lett. **92**, 042002 (2004) [arXiv:hep-ph/0304249].

[13] Ph. Hägler *et al.* [LHPC Collaborations], Phys. Rev. D **77** (2008) 094502 [arXiv:0705.4295 [hep-lat]].

[14] R. L. Jaffe and A. Manohar, Nucl. Phys. B **337**, 509 (1990).

[15] X. D. Ji, J. Tang and P. Hoodbhoy, Phys. Rev. Lett. **76** (1996) 740 [arXiv:hep-ph/9510304].

[16] X. D. Ji, Phys. Rev. Lett. **78** (1997) 610 [arXiv:hep-ph/9603249].

[17] M. Burkardt, A. Miller and W. D. Nowak, Rept. Prog. Phys. **73**, 016201 (2010) [arXiv:0812.2208 [hep-ph]].

[18] M. Wakamatsu, Phys. Rev. D **81**, 114010 (2010) [arXiv:1004.0268 [hep-ph]].

[19] R. L. Jaffe, Phys. Lett. B **365**, 359 (1996) [arXiv:hep-ph/9509279].

[20] M. Alekseev *et al.* [COMPASS Collaboration], Phys. Lett. B **676** (2009) 31 [arXiv:0904.3209 [hep-ex]].

[21] A. Airapetian *et al.* [HERMES Collaboration], arXiv:1002.3921 [hep-ex].

[22] A. J. Buras, Rev. Mod. Phys. **52** (1980) 199.

[23] E. G. Floratos, D. A. Ross and C. T. Sachrajda, Nucl. Phys. B **152** (1979) 493.

[24] S. A. Larin, T. van Ritbergen, J. A. M. Vermaseren, Nucl. Phys. **B427** (1994) 41-52.

[25] S. A. Larin, P. Nogueira, T. van Ritbergen *et al.*, Nucl. Phys. **B492** (1997) 338-378. [hep-ph/9605317].

[26] A. Retey and J. A. M. Vermaseren, Nucl. Phys. B **604** (2001) 281 [arXiv:hep-ph/0007294].

[27] M. Wakamatsu and Y. Nakakoji, Phys. Rev. D **77** (2008) 074011 [arXiv:0712.2079 [hep-ph]].

[28] G. 't Hooft, Nucl. Phys. B **61** (1973) 455.

[29] W. A. Bardeen, A. J. Buras, D. W. Duke and T. Muta, Phys. Rev. D **18** (1978) 3998.

[30] R. Mertig and W. L. van Neerven, Z. Phys. C **70** (1996) 637 [arXiv:hep-ph/9506451].

[31] W. Vogelsang, Phys. Rev. D **54** (1996) 2023 [arXiv:hep-ph/9512218].

[32] A. Vogt, S. Moch, M. Rogal and J. A. M. Vermaseren, Nucl. Phys. Proc. Suppl. **183** (2008) 155 [arXiv:0807.1238 [hep-ph]].

[33] Ph. Hägler, Phys. Rept. **490**, 49 (2010) [arXiv:0912.5483 [hep-lat]].

[34] J. D. Bratt *et al.* [LHPC Collaboration], Phys. Rev. **D82** (2010) 094502. [arXiv:1001.3620 [hep-lat]].

[35] M. Dorati, T. A. Gail and T. R. Hemmert, Nucl. Phys. A **798**, 96 (2008) [arXiv:nucl-th/0703073].

[36] S. Bethke, Eur. Phys. J. **C64** (2009) 689-703. [arXiv:0908.1135 [hep-ph]].

[37] K. Nakamura *et al.* [Particle Data Group Collaboration], J. Phys. **G37** (2010) 075021.

[38] D. V. Shirkov and I. L. Solovtsov, Phys. Rev. Lett. **79** (1997) 1209 [arXiv:hep-ph/9704333].

[39] C. S. Fischer, R. Alkofer, Phys. Rev. **D67** (2003) 094020. [hep-ph/0301094].

[40] G. M. Prosperi, M. Raciti, C. Simolo, Prog. Part. Nucl. Phys. **58**, 387-438 (2007). [hep-ph/0607209].

[41] A. W. Thomas and W. Weise, "The Structure of the Nucleon," *Berlin, Germany: Wiley-VCH (2001) 389 p*

[42] A. W. Thomas, Adv. Nucl. Phys. **13** (1984) 1.

[43] S. Theberge and A. W. Thomas, Nucl. Phys. A **393** (1983) 252.

[44] A. Chodos, R. L. Jaffe, K. Johnson and C. B. Thorn, Phys. Rev. D **10** (1974) 2599.

[45] S. D. Bass, A. W. Thomas, Phys. Lett. **B684** (2010) 216-220. [arXiv:0912.1765 [hep-ph]].

[46] T. A. DeGrand, R. L. Jaffe, K. Johnson and J. E. Kiskis, Phys. Rev. D **12** (1975) 2060.

[47] M. Schumann, R. J. Lindebaum and R. D. Viollier, Eur. Phys. J. C **16** (2000) 331.

[48] H. Hogaasen and F. Myhrer, Phys. Rev. D **37** (1988) 1950.

[49] F. Myhrer and A. W. Thomas, Phys. Rev. D **38** (1988) 1633.

[50] J. Wroldsen and F. Myhrer, Z. Phys. C **25** (1984) 59.

[51] R. D. Viollier, S. A. Chin and A. K. Kerman, Nucl. Phys. A **407** (1983) 269.

[52] M. Wakamatsu, Eur. Phys. J. A **44** (2010) 297 [arXiv:0908.0972 [hep-ph]].

17